The Discontinuous Weld Bead Defect in High-Speed Gas Metal Arc Welds

A new type of high-speed gas metal arc weld bead defect was observed and characterized

BY T. C. NGUYEN, D. C. WECKMAN, AND D. A. JOHNSON

ABSTRACT. A common weld bead defect that occurs at high fusion welding speeds is the periodic undulation of the weld bead profile, also known as humping. In the present study, when using argon shielding gas, 0.9-mm-diameter ER70S-6 and ER70S-3 electrode wires, and welding powers between 9 and 12 kW during high-speed gas metal arc welding of SAE-AISI 1018 cold rolled steel plate, swinging spray metal transfer was observed and the welding speed was found to be limited to 15 mm/s by the onset of the periodic humping phenomenon. However, rotational metal transfer was observed when using reactive shielding gases at these powers and the welding speed was limited to 22 mm/s by the onset of a new, as yet unreported, weld defect that was distinctly different from humping. This new high-speed defect is referred to as the discontinuous weld bead defect, since the defective weld bead is broken up into several good bead segments by aperiodic or irregularly spaced valleys or depressions where melting of the base metal occurred but no filler metal was deposited. The results also indicated that nominal electrode wire composition did not appear to play a significant role in the formation of the humping or the discontinuous weld bead defects.

A LaserStrobe™ video imaging system was used to obtain video images of typical sequences of events during the formation of the humping and discontinuous weld bead defects. From these images, the discontinuous weld bead defect was found to be caused by the inconsistent, aperiodic deposition of molten filler metal during rotational filler metal transfer mode when using reactive shielding gases. The long molten filler metal string on the end of the electrode wire was erratically fragmented and required time to re-form prior to the resumption of the transfer of filler metal. The temporary disruption of filler metal deposition created a filler-metal-free depression that broke up the otherwise good weld bead, thereby forming the discontinuous weld bead defect. The irregular fragmentation of the molten filler metal string during rotational transfer and subsequent formation of the aperiodic discontinuous weld bead defect are phenomena that have not previously been observed or reported in the open literature.

T. C. NGUYEN was with the University of Waterloo. He is now at the School of Engineering and Information Technology, Conestoga College, Kitchener, Ont., Canada. D. C. WECKMAN and D. A. JOHNSON are with the Department of Mechanical Engineering, University of Waterloo, Waterloo, Ont., Canada.

Introduction

Welding is a ubiquitous process and an integral part of most manufacturing industries such as the construction, shipbuilding, aerospace, automotive, petrochemical, and electronics industries. To remain competitive in today's manufacturing environment, companies must continuously improve their productivity without sacrificing the quality of their products. Increases in productivity will reduce overall production costs, thereby maintaining and strengthening the company's competitiveness. Overall production costs can usually be reduced by evaluating the productivity of the welding processes used. For many welded products, an increase in productivity often requires use of higher welding speeds. Frequently, this can be achieved through optimizing or automating existing welding processes. In certain cases, switching to newer high-energy-density welding processes will also result in higher welding speeds and increases in productivity.

KEYWORDS

Gas Metal Arc Welding
Humping
Weld Defects
Argon Shielding Gas
Reactive Shielding Gases
Discontinuous Weld Beads
Carbon Steel

In order to weld at higher welding speeds, the heat input of all fusion welding processes must be increased to maintain the same amount of energy input per unit length of weld required for melting of filler and base metals (Refs. 1–3), otherwise, the weld cross section will decrease and eventually no melting of the base metal will occur. While increasing welding speed and heat input will provide the desired productivity increase, continued increases of the welding speed is in practice limited by the deterioration of the quality of weld bead profile. One of the most commonly occurring geometric defects that has been observed at high welding speeds is the humping phenomenon (Refs. 4–6). An example of a humped gas metal arc (GMA) weld bead is shown in Fig. 1. Humping can be described as a periodic undulation of the weld bead with regularly spaced humps and valleys. Figure 2 shows transverse sections at a valley and a hump, respectively, of the humped GMA weld bead in Fig. 1. Although the depth of penetration is the same for both transverse sections, there is more weld metal accumulation at the hump. The humping defect compromises the mechanical integrity of the weld joint, thereby limiting the welding speed and thus overall production rates.

Nguyen et al. (Ref. 5) and Soderstrom and Mendez (Ref. 6) have recently reviewed the literature related to high-speed fusion weld bead defects, their causes, and techniques that have been used to increase welding speed. Humping of the weld bead has been the most commonly observed high-speed weld defect. It has been reported to occur in both nonautogenous welding processes, such as GMA welding (Refs. 7–9) and autogenous processes such as gas tungsten arc (GTA) welding (Refs. 10, 11), laser beam welding (LBW) (Refs. 12, 13), and electron beam welding (EBW) (Refs. 14–16).

Bradstreet (Ref. 7) was the first to report the formation of humped welds during GMA welding of plain carbon steel using spray transfer mode. He found that

the humping phenomenon is periodic and influenced by the welding speed, the welding voltage, the angle of the electrode with respect to the workpiece, and other parameters. He also observed that reactive shielding gases such as Ar-CO_2 and Ar-O_2 mixes significantly increased the limiting welding speed before humping occurred and argued that this was a result of the lower surface tension and improved wetting that occurred when the reactive gases were used. In later studies, Nishiguchi et al. (Refs. 8, 9) developed a parametric map of arc voltage vs. welding speed for GMA welding of mild steel using short circuit metal transfer mode while Nguyen et al. (Ref. 17) used Ar and two reactive shielding gases and spray transfer mode to create a map of GMA welding power versus welding speed. These parametric maps showed regions of process parameters that produced good weld beads and regions that resulted in humping and other weld bead defects. In both cases, they found that humping occurred as the welding speed was increased above a certain critical welding speed and that there was an inverse relationship between this critical welding speed and the welding voltage or power used, i.e., as the welding voltage or power was increased, humping occurred at lower welding speeds.

In autogenous welding processes, humping has been found to be periodic and influenced by welding process parameters such as welding speed, welding power, type of shielding gas, ambient pressure, electrode geometry, travel angle, and energy density at the workpiece, etc. (Refs. 10–16). Several attempts have been made to express the relationship between these process variables and the onset of humping (Refs. 7–21). Typically, these included process maps that show the onset of humping with respect to welding speed and welding current or welding power. On each of these process maps, welding process parameters such as the shielding gas composition, the torch angle, or the GTA electrode geometry are normally kept constant.

Several models of the periodic humping phenomenon have been proposed. These include the Rayleigh Jet Instability model first proposed by Bradstreet (Ref. 7) and its modifications by Gratzke et al. (Ref. 22), the Arc Pressure model by Paton et al. (Ref. 23), and the Supercritical Flow model by Yamamoto and Shimada (Ref. 10). In a subsequent study of humping during GTA welding of stainless steel, Mendez and Eagar (Refs. 19–21) argued that humping was caused by periodic premature solidification of the thin liquid film at the bottom of the arc gouged region of the weld pool. This choked off flow of molten metal to the back of the weld pool and resulted in the initiation of a new hump further along the weld bead. These models suggest that fluid flow, arc pressure, metallostatic pressure, capillary force, and lateral instability of a cylindrical jet of molten weld metal and premature solidification of the thin film of molten metal in the arc gouged region of the weld pool are all possible factors responsible for the periodic humping phenomenon.

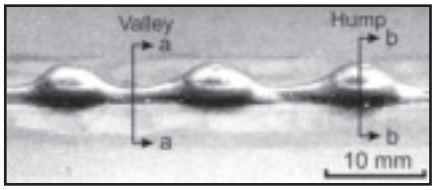

Fig. 1 — A bead-on-plate GMA weld in plain carbon steel exhibiting the humping weld bead defect.

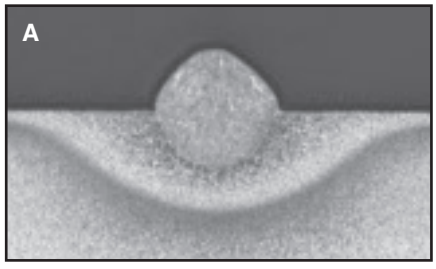

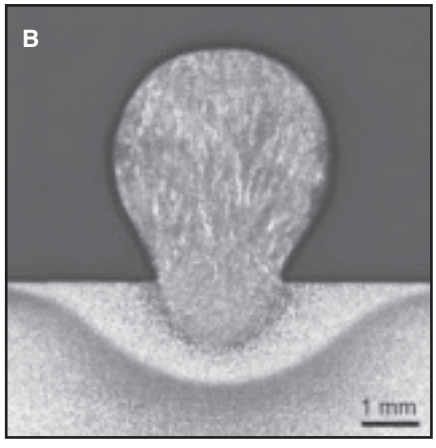

Fig. 2 — Transverse sections of the GMA weld shown in Fig. 1 at the following: A — A valley, and B — a hump.

Based on video imaging of GMA welds made on mild steel plates and corroborating experiments, Nguyen et al. (Refs. 5, 17) have recently proposed a curved wall jet model of humping in nonautogenous welding processes such as GMA welding. Figure 3 shows a schematic diagram of this model of humping in high-speed GMA welding. As the welding speed increases, the weld pool becomes elongated, shallow, and narrow. Also, the electrode, the welding arc, and the metal droplet stream move forward and closer to the leading edge of the weld pool, i.e., the longitudinal distance from the leading edge of the weld pool to the location where the filler metal droplet impinges the top surface of the weld pool, d, decreases. The combined actions of the arc force and the droplet momentum create a depression or gouged region at the front of the weld pool that contains a thin layer of liquid metal underneath the welding arc. In addition, the filler metal droplets hit the sloping leading edge of the weld pool and this molten filler metal is then redirected toward the tail of the weld pool at high velocity through a semicircular curved wall jet similar in shape to the valley portion of the humped weld bead shown in Figs. 1 and 2A, dragging with it any liquid metal in the front of the weld pool from the melting base metal. At the tail of the weld pool in Fig. 3, the molten weld metal accumulates to form a swelling that is drawn into a spherical bead shape by surface tension (see humps in Figs. 1 and 2B) as molten metal is fed into the swelling from the front of the weld pool through the wall jet. As the welding arc continues to move to the left along the weld joint, the wall jet shown in Fig. 3 becomes increasingly elongated and the thermal mass of molten metal inside the wall jet becomes distributed over a longer distance until continued solidification of the weld and the molten metal in the elongated wall jet chokes off the flow of molten metal to the swelling. Solidification of the wall jet illustrated in Fig. 3 forms the valley typically observed between swellings in a humped GMA weld bead such as those shown in Figs. 1 and 2A. Initiation and growth of a new swelling closer to the arc and further along the weld bead occurs very soon after fluid flow in the wall jet is choked off. This sequential formation of a swelling or hump at the tail of the weld pool and solidification of the wall jet is a periodic phenomenon where the humping

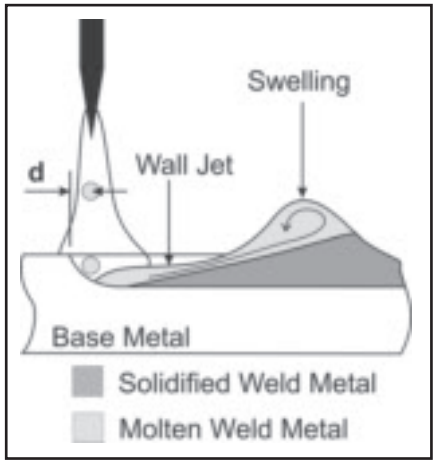

Fig. 3 — The curved wall jet model for the periodic humping phenomenon during high-speed GMAW (after Nguyen et al. (Refs. 5, 17)).

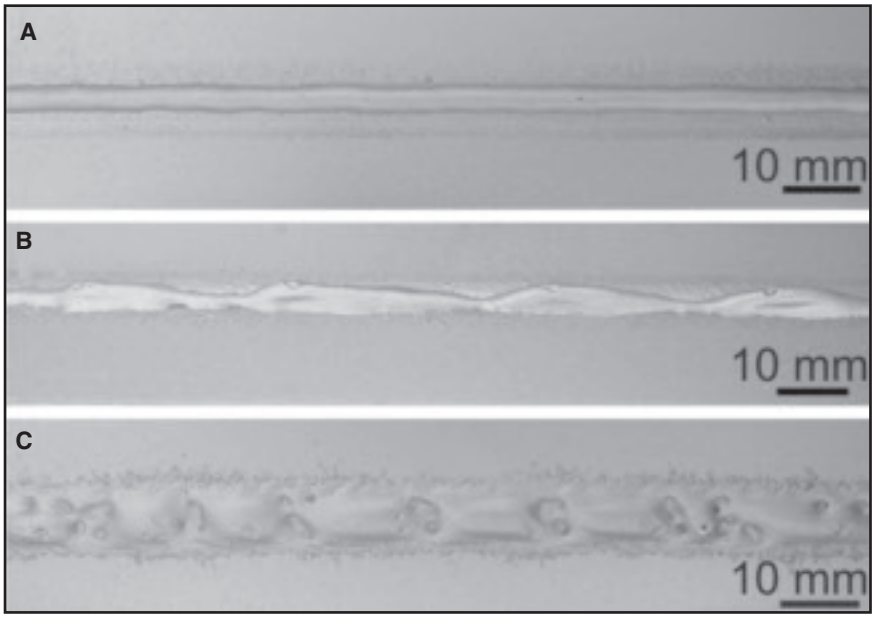

Fig. 4 — Top view of GMA welds produced using a reactive shielding gas, 40 mm/s welding speed. A — 6 kW; B — 8 kW; and C — 11 kW welding power.

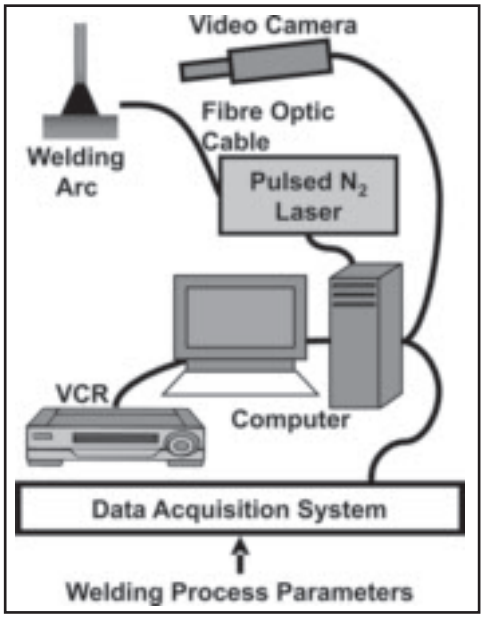

Fig. 5 — A schematic diagram showing various components of the LaserStrobe™ video imaging system.

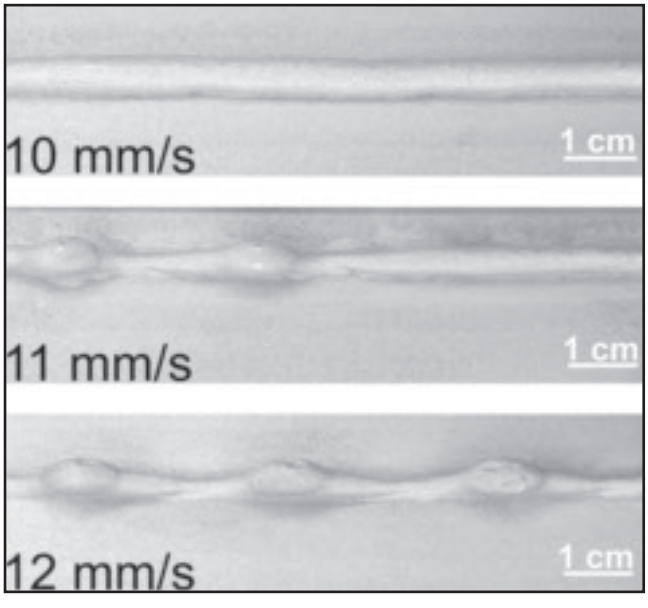

Fig. 6 — Top view of GMA welds produced using 6.3 kW welding power, argon shielding gas, and at various welding speeds.

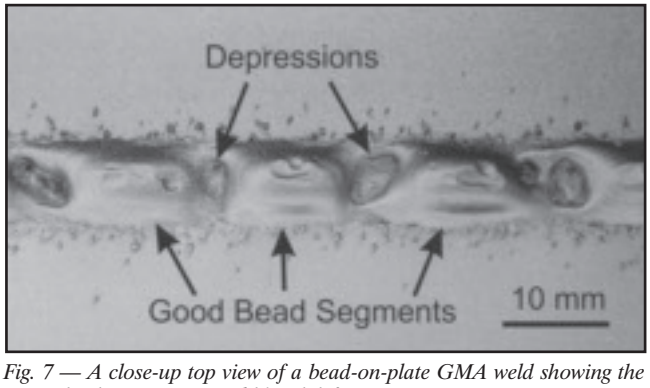

Fig. 7 — A close-up top view of a bead-on-plate GMA weld showing the aperiodic discontinuous weld bead defect.

frequency has been shown to increase with increasing welding speed or decreasing welding power (Ref. 24).

During their study of the humping phenomena in high-speed GMA welding of plain carbon steel, Nguyen et al. (Refs. 5, 17, 24) observed a change in the humped weld bead morphology when welds were performed using reactive shielding gases and welding powers greater than 9 kW. Figure 4 shows three GMA welds that were produced at 40 mm/s welding speed using a reactive shielding gas and increasing welding powers of 6, 8, and 11 kW. These welds have been cleaned by sandblasting to clearly reveal the different geometric features of the bead. As shown in Fig. 4A, a good GMA weld was produced when using 6 kW welding power and humping was observed when the welding power was increased to 8 kW — Fig. 4B. However, as shown in Fig. 4C, when the welding power was further increased to 11 kW, the GMA weld produced showed a distinctly different type of geometric weld defect that is clearly not humping. The regular, periodic behavior of humping was no longer evident and the curved wall jet in the valleys of the high-speed weld bead defect was no longer present. This new high-speed defect is referred to here as the discontinuous weld bead defect, because the defective weld bead as shown in Fig. 4C is broken up into several good bead segments by aperiodic or irregularly spaced valleys or depressions where melting of the base metal occurred but no filler metal was deposited. In addition, while the normally observed decrease in critical welding speed with increasing welding power was evident at the lower powers when humping occurred, the critical welding speed was not affected by the welding power when this new weld bead defect was observed. This particular aperiodic high-speed GMA weld bead defect has not been previously identified or reported in the literature (Refs. 1–5, 17, 24). The objectives of the present study (Ref. 24), therefore, were to observe, identify, experimentally validate, and understand the physical mechanisms responsible for this new discontinuous weld bead defect that occurred during high-speed GMA welding of plain carbon steel.

Experimental Apparatus and Procedures

In the present study, bead-on-plate GMA welds were made using a Fanuc ARC Mate 120i 6-axis welding robot and a Lincoln PowerWave™ 455 power supply operating in constant voltage mode with an integrated Power Feed 10 wire feeder over a wide range of preset welding speeds and welding powers. A PC-microcomputer was used with *Labview*™ software and National Instruments™-based data-acquisition system to record the welding voltage and current. Voltage between the contact tip and the workpiece was measured at the rate of 1000 samples/s using a LEM™ LV100 voltage transducer and the welding current was measured using a LEM™ LT505-S current transducer. The measured voltages, V (V), and currents, I (A), were then postprocessed to calculate the time averaged welding power, P (W), using $P = V \times I$.

A LaserStrobe™ video system (Ref. 25) was used to observe and to record images of the humping phenomenon during bead-on-plate GMA welding of plain carbon steel plate. As shown schematically in Fig. 5, the LaserStrobe™ video imaging system consisted of a video camera, a video recorder (VCR), a pulsed nitrogen (N_2) laser strobe with fiber-optic beam delivery, a data-acquisition system, and a personal computer that acted as a system controller. The pulsed N_2 laser strobe was used to overwhelm the intense radiation of the GMA welding arc since the laser light was much brighter than the light coming from the welding arc at the N_2 laser wavelength (Ref. 25). The laser-illuminated scene was viewed by a video camera equipped with a CCD video sensor, a narrow band-pass filter centered on the 337.1-nm wavelength of the N_2 laser, and an image intensifier that was also used as a high-speed electronic shutter. The image intensifier limits the resolution of the LaserStrobe™ image to about 420 line pairs in the horizontal direction (Ref. 25). The computer synchronized the camera's electronic shutter with the laser pulses. The combination of temporal filtering provided by the electronic shutter, N_2 laser pulse synchronization, and spectral filtering from the narrow band-pass filter allowed unobstructed viewing of the events taking place during the formation of humped GMA welds without the intense light from the welding arc. During filming, the video camera was mounted on a fixture that moved along with the GMA welding torch.

All bead-on-plate GMA welds were made in the flat position on degreased 6.5-mm- (¼-in.-) thick cold-rolled SAE-AISI 1018 plain carbon steel plates using 0.9-mm- (0.035-in.-) diameter ER70S-3 and ER70S-6 electrode wires and a 22-mm contact tip-to-workpiece distance. The majority of GMA welding experiments were performed using ER70S-6 electrode wire. However, ER70S-3 electrode was also employed to determine the effects of the differences in chemical composition of the filler metal on the formation of high-speed weld defects. The nominal chemical compositions of these GMAW electrode wires are as listed in Table 1 (Ref. 3). Both of these electrodes have relatively high levels of the deoxidizing elements, Mg and Si. The ER70S-6 electrode wire has the highest concentrations of Mg and Si and is often recommended for applications that use high welding current or GMAW over steel plates that are covered with light rust, whereas the ER70S-3 electrode is recommended when welding clean steel with argon-based shielding gases (Ref. 3). In all cases, the working angle of the GMAW gun was 90 deg and the travel angle was 0 deg.

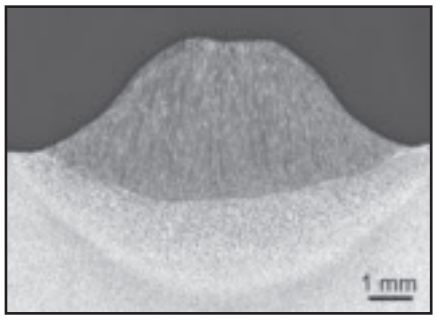

Fig. 8 — A photomicrograph showing the transverse section of a good bead segment of a GMA weld with discontinuous defect. The weld was produced using TIME™ shielding gas, 10 kW welding power, and 30 mm/s welding speed.

Three different welding-grade shielding gases were used: argon, Mig Mix Gold™ (MMG™[1]) and TIME™[2]. The composition of each shielding gas is listed in Table 2. In this study, argon was an inert shielding gas while MMG™ and TIME™ were reactive shielding gases due to their oxygen (O_2) and carbon dioxide (CO_2) contents.

To determine the usable welding speeds at each power level, the weld bead profiles were examined and the maximum welding speed that produced a non-humped or acceptable weld bead was recorded. For example, Fig. 6 contains photographs showing the top view of GMA welds produced using 6.3 kW welding power, argon shielding gas, and 10, 11, and 12 mm/s welding speeds, respectively. In Fig. 6, the welds produced at 10 mm/s welding speeds or slower were classified as good welds, since the weld beads show no significant variation in weld dimensions or shape along the length of the weld. However, at 11 mm/s welding speed, the weld bead begins to exhibit intermittent swellings that are separated by valleys. The occurrence of the humps and valleys becomes consistently periodic at 12 mm/s welding speed. Thus, the difference between good weld beads and a humped weld can be clearly identified by the significant variations in weld bead dimensions and shape that occur along the length of the humped weld bead and the occurrence of regularly spaced humps and valleys. Based on the weld beads shown in Fig. 6, the limiting welding speed for production of good argon-shielded GMA welds using 6.3-kW welding power was 10 mm/s. This procedure was also used to determine the critical or maximum welding speed that could be used before the newly identified discontinuous weld bead defect became evident.

Table 1 — The Nominal Chemical Compositions of ER70S-3 and ER70S-6 Electrode Wires in wt-% (Ref. 3)

	Carbon	Manganese	Silicon
ER70S-3	0.06–0.15	0.90–1.40	0.45–0.70
ER70S-6	0.07–0.15	1.40–1.85	0.80–1.15

Note: Phosphorus 0.025 max. and Sulfur 0.035 max.

Table 2 — Compositions of the GMAW Shielding Gases Used

Shielding Gas	Composition
Argon	100% Ar (ultrahigh purity grade)
MMG™	92% Ar, 8% CO_2
TIME™	65% Ar, 8% CO_2, 26.5% He, 0.5% O_2

Results and Discussion

Geometric Features of the Discontinuous Weld Bead Defect

As the welding power was increased from 5 to 9 kW, the onset of high-speed weld defects in GMA welds produced using the reactive shielding gases occurred at lower welding speeds. The high-speed weld defect observed was primarily humping. The results of these experiments and an explanation of the periodic humping phenomenon in high-speed GMA welding are reported in detail in a previous article by Nguyen et al. (Ref. 17). However, at welding powers greater than 9 kW, the filler metal transfer mode in the GMAW process was observed to change from

1. MMG™, Praxair Distribution, Inc., Kitchener, Ont., Canada.

2. TIME™, BOC Gases Canada Ltd., Waterloo, Ont., Canada.

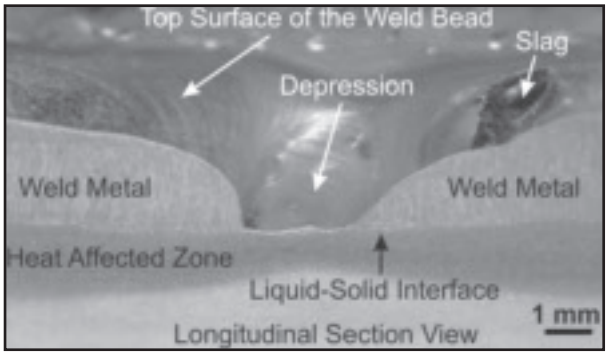

Fig. 9 — Top and longitudinal section views at the depression of a GMA weld with a discontinuous weld bead defect. The weld was produced right to left using 10 kW welding power, TIME™ shielding gas, and 30 mm/s welding speed.

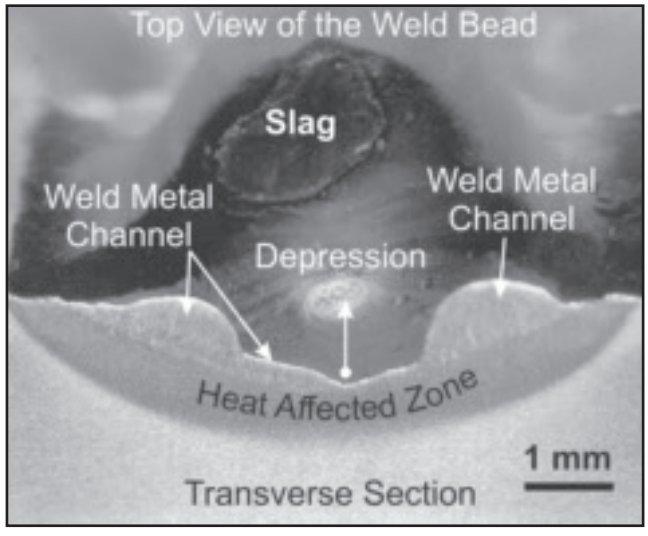

Fig. 10 — The transverse section and the top view at the depression of a GMA weld with discontinuous weld bead defect. The weld was made using 10 kW welding power, TIME™ shielding gas, and 30 mm/s welding speed.

spray to rotational transfer and there was a distinct change in the weld bead morphology as shown in Fig. 4C.

Figure 7 shows a close-up top view of the aperiodic discontinuous weld bead defect. This particular weld was produced using 10 kW welding power, 30 mm/s welding speed, and TIME™ shielding gas. Again, the top surface of the weld has been cleaned by sandblasting to reveal all features of the weld. The weld bead is not continuous but is broken up into segments of good weld bead by irregularly spaced depressions. As may be seen in Fig. 7, the adjacent good weld bead segments are connected by small metal channels on the outer edge of the depression. In addition, the discontinuous weld bead exhibits a significant amount of weld spatter immediately adjacent to the weld bead.

A transverse section across a good bead segment of a discontinuous weld bead defect is shown in Fig. 8. This weld segment has a bead profile that shows good penetration, wide width, and excellent wetting with the original surface of the workpiece. At the deepest point, the depth of penetration is approximately 1 mm. There is no evidence of the characteristic finger penetration or nail-head weld profile that was typical of the welds produced using spray transfer at welding powers less than about 9 kW (Ref. 17).

Figure 9 shows the top and the longitudinal section views of a GMA weld with the discontinuous weld bead defect from the end of one good weld segment across the depression to the beginning of another good weld segment. The welding direction was from the right to left. The depression shown in Fig. 9 can be described as a cavity or a sunken valley between two good weld segments following closely the shape of the fusion boundary. The fusion boundary of the depression has the same depth of penetration as the good weld bead segments. However, unlike the good segments of the weld bead, the depression has a shallower heat-affected zone (HAZ), which is delineated by the dark band immediately located below the fusion boundary — Fig. 9. In this photomicrograph, the HAZ of the weld was revealed by etching the polished longitudinal section with a 5% Nital solution (Ref. 26). The shallower HAZ is an indication that the total amount of heat input was less at the depression compared to that along the good segments of the defective weld. This would suggest that the lack of the weld metal at the depression reduced the amount of sensible heat input into the base metal, thereby decreasing the size of the HAZ.

The good weld bead segment on the right side of Fig. 9 has a gradual forward-sloping profile in the direction of welding. As indicated, there is a slag particle on the top surface of the weld bead prior to the depression. Based on energy dispersive X-ray (EDX) analysis, this was a $(Mn,Si)_xO_y$ glassy slag with about 7 at.-% Mn, 17 at.-% Si, and 74 at.-% O with trace amounts of Fe and Al. These features were typically seen at the end of GMA welds produced using the reactive shielding gases. Meanwhile, beyond the depression, the start of the next weld bead segment did not have good wetting with the bottom surface of the weld pool, since its contact angle is very close to 90 deg ($\pi/2$ radians). These geometric features suggest that a momentary stoppage in the transfer of filler metal had occurred during welding, since these two adjacent weld bead segments appear to be the end of one and the beginning of another GMA weld bead.

To further examine the features of the depression, Fig. 10 shows a transverse section of a discontinuous GMA weld made using 10 kW welding power, TIME™ shielding gas, and 30 mm/s welding speed. The transverse section was etched with 5% Nital solution. In this photograph, the specimen was tilted forward to reveal the transverse section as well as the top view of the depression and the view is toward the tail of the weld. As indicated in Fig. 10, there is a patch of $(Mn,Si)_xO_y$ slag on the top surface of the previous good weld segment. Also, inside the cavity of the depression, there appears to be a very thin layer of solidified weld metal. This is consistent with observations made by Yamamoto and Shimada (Ref. 10) and later by Mendez et al. (Refs. 19–21) of gouged weld pools during high-speed autogenous GTA welding of stainless steel.

From the transverse section of the weld shown in Fig. 10, the HAZ is uniform in thickness at the depression. In addition, there are two solidified channels or wall jets on both sides of the depression near the upper rim. These weld metal wall jets connect the adjacent good segments of the discontinuous weld bead defect. These solidified weld metal channels or wall jets are similar to those observed by Mendez et al. (Refs. 19–21) in their GTA welds. Since the molten weld metal flows around the rim of the depression and there is a thin layer of molten weld metal within the depression, high arc pressure must have been present inside the depression during welding. This geometric feature is very similar to that produced during the high-power autogenous GTAW process, especially at high welding speeds. These observations suggest that during the time when the depression is created in the discontinuous weld bead, the GMA welding process behaves like an autogenous welding process with little or no filler metal transferred from the electrode to the workpiece.

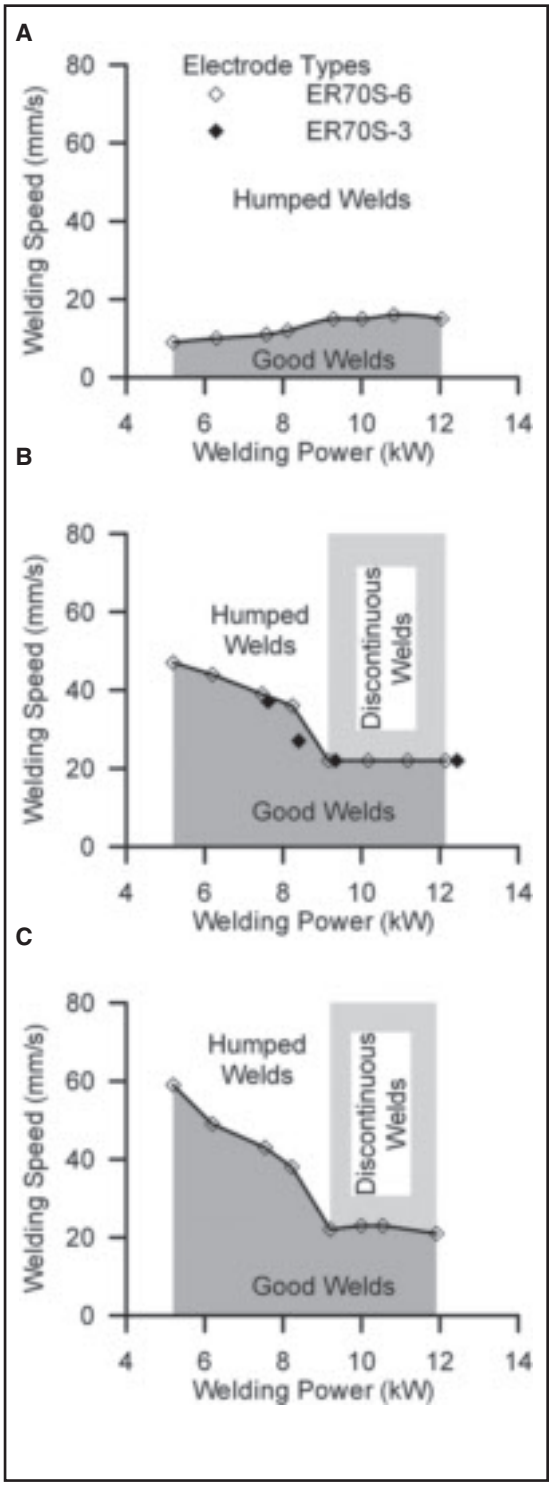

Fig. 11 — Regions of good and defective weld beads on welding speed vs. welding power plot for — A — Argon, B — MMG™, and C — TIME™ shielding gases.

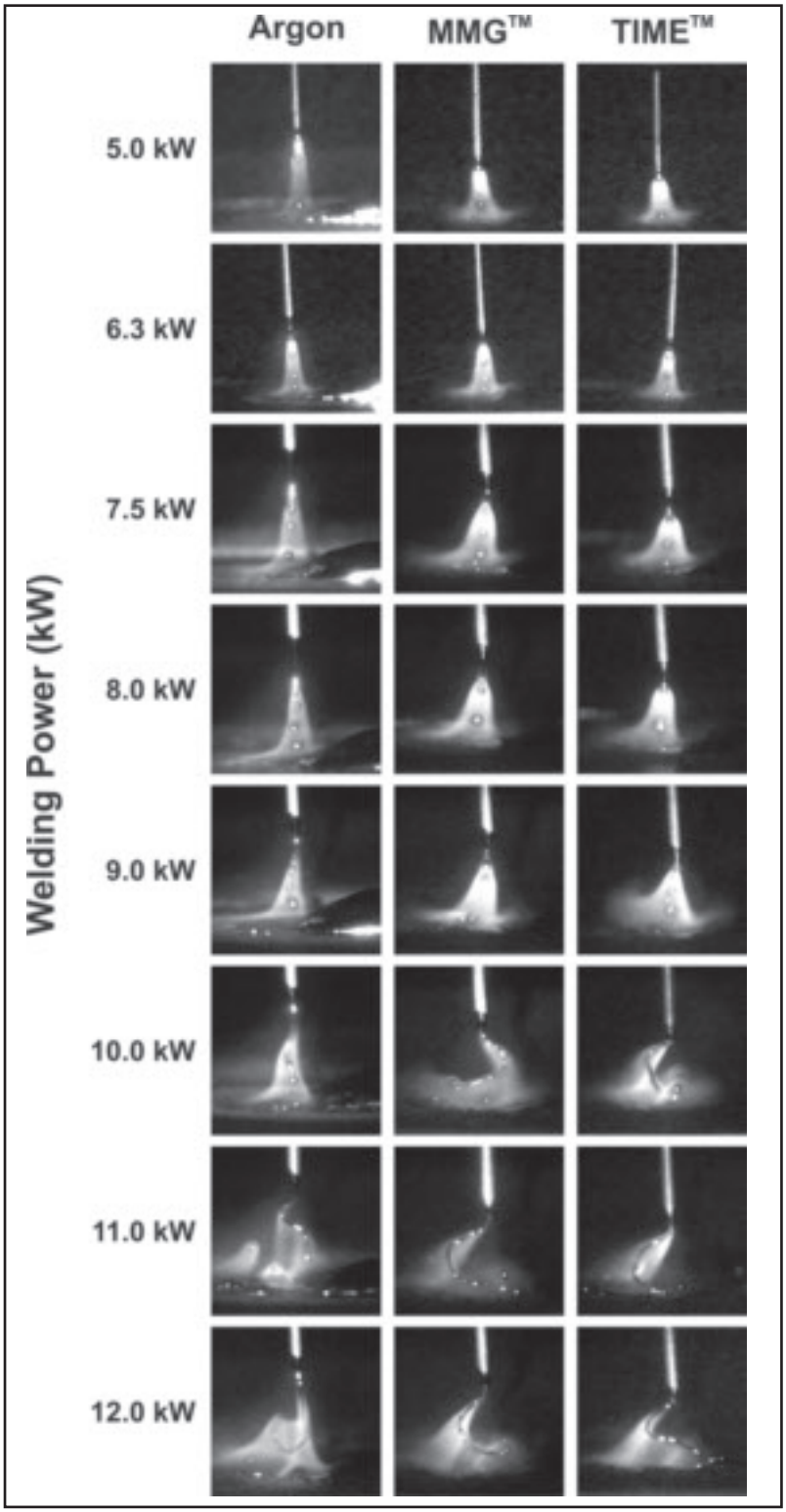

Fig. 12 — The filler metal transfer modes as a function of the welding powers and shielding gases. In these images, the diameter of the filler metal electrode wire is 0.9 mm.

Effects of Welding Power and Welding Speed

In a previous study of the humping phenomenon in GMA welding, the total welding power used was varied from 5 to 9 kW (Ref. 17). In the present study of the discontinuous weld bead defect, however, the total welding power was increased further to 10, 11, and 12 kW. For each different combination of welding power and shielding gas, the previously described experimental procedure for determining the limiting welding speed was performed. The new limiting welding speeds generated from these experiments were then combined with previous data and plotted.

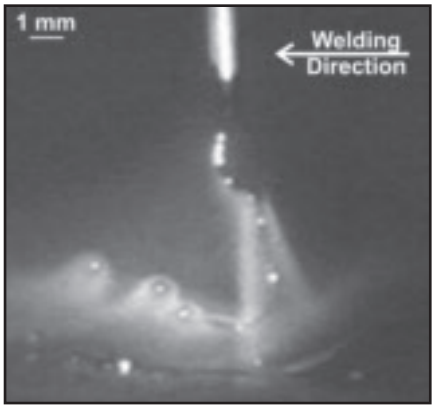

Fig. 13 — The flight path of molten filler metal droplets in rotational transfer mode at 11 kW using argon shielding gas.

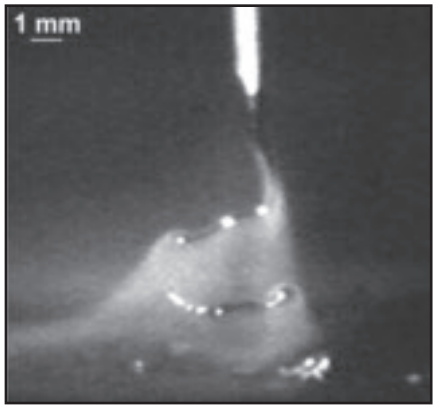

Fig. 14 — An image of rotational transfer mode produced using argon shielding gas and 12 kW welding power showing the detachment of a long string fragment from the molten filler metal string.

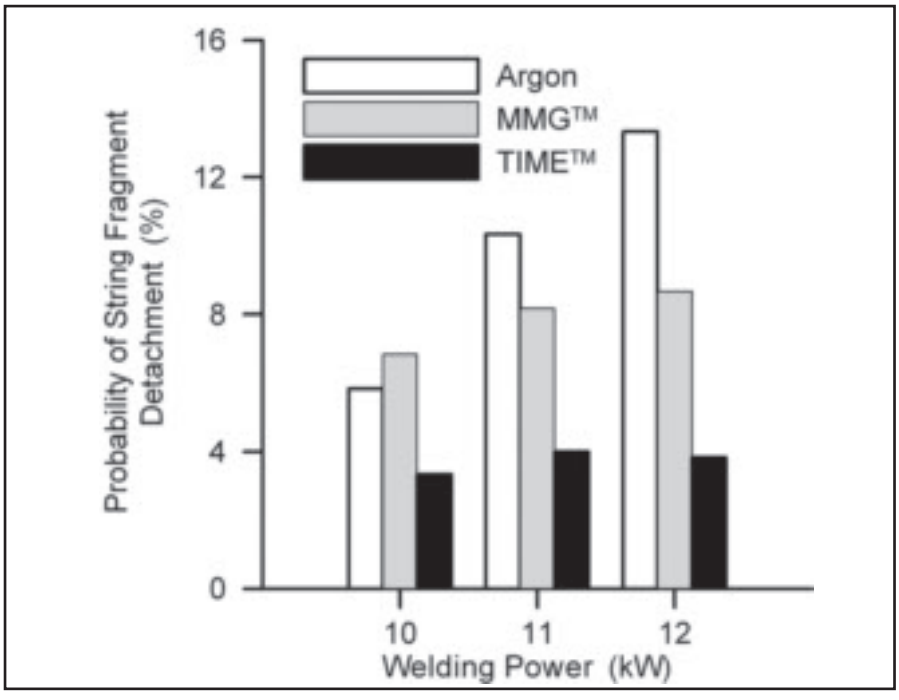

Fig. 15 — The relative frequency of the breakup of the molten filler metal string at three different welding power levels and three different shielding gases.

The three graphs displayed in Fig. 11 are process maps showing regions or ranges of welding power and welding speed that resulted in good and defective weld beads when using the three different shielding gases: argon, MMG™, and TIME™. On these plots, the connecting line segments represent the maximum or limiting welding speeds that could be used to produce a GMA weld without a defective weld bead profile. The area located directly underneath the limiting welding speeds represents various combinations of welding speed and welding power that produced good or acceptable GMA weld beads. For convenience, these areas are labeled as good weld regions on the plots. As the speed is increased beyond the limiting welding speeds, a geometrically defective or unacceptable weld bead was observed. Note that the limiting welding speeds and the types of high-speed weld defect for GMA welds produced using MMG™ shielding gas and ER70S-3 electrode wire are also plotted in Fig. 11B. As may be seen in Fig. 11, there were two types of geometric weld bead defects observed at higher welding speeds: humped and discontinuous weld beads as shown in Fig. 6B and C, respectively. The type of high-speed weld defect observed was a function of the shielding gas and the welding power used to make the weld. In addition, there is no significant difference between the results when ER70S-3 or ER70S-6 electrode wires were used with MMG™ shielding gas.

When using both the MMG™ and TIME™ shielding gases and less than 9 kW welding power, the usable welding speed was limited by the occurrence of humping. In this range of welding power, as the welding power was increased, humping occurred at lower welding speeds — Fig. 11B, C. When using lower welding powers and TIME™ shielding gas, defect-free welds were produced at slightly higher welding speeds than those made using MMG™ shielding gas. However, this advantage diminished with increasing welding power. On the other hand, when using argon shielding gas, there was a small increase in limiting welding speeds with higher welding powers. This limiting welding speed increase when using Ar shielding gas was thought to be due to the effects of the transition from streaming to swinging spray transfer modes of the filler metal on the humping phenomenon (Ref. 17).

When the welding power was increased beyond 9 kW, the limiting welding speed for welds produced using the argon shielding gases leveled out at approximately 15 mm/s and became independent of the welding power — Fig. 11A. The same trend was also observed for GMA welds produced using the reactive shielding gases, MMG™ and TIME™; however, the limiting welding speeds were greater at approximately 22 mm/s — Fig. 11B, C. As indicated in Fig. 11A–C, as the welding power was increased beyond 9 kW when using argon shielding gas, the observed high-speed weld defect was still humping, whereas when using the reactive shielding gases, the usable welding speed was limited by the onset of the discontinuous weld bead defect. In addition, there was a distinct point of inflection between the limiting welding speed lines for humping versus the discontinuous weld bead defect. This point of inflection and change in behavior at welding powers greater than 9 kW is indicative that a transition has taken place in the physical phenomena taking place during GMA welding such as a change in the filler metal transfer mechanism. The filler metal transfer mode in the GMA welding process is known to change from globular to spray and finally to rotational transfer with increasing welding power (Ref. 4). In the following, therefore, the relationship between the filler metal transfer modes and the welding power levels is explored.

The Filler Metal Transfer Modes

Individual LaserStrobe™ video frames showing the typical filler metal transfer

modes observed when using the different shielding gases and welding powers are shown in Fig. 12. The welds produced using argon shielding gas had the longest arc length of about 9 mm whereas the welds produced using MMG™ and TIME™ shielding gases were typically about 50% shorter. Between welding powers of 5 and 7.5 kW, the spray transfer mode is evident for all shielding gases. At these welding power levels, the molten filler metal droplets detached from the end of the electrode wire and were propelled straight down through the welding arc to the weld pool. The molten filler metal droplets for the argon shielding gas was found to have a more constricted flight path resulting in a smaller impingement area on the top surface of the weld pool (Ref. 17). Meanwhile, the molten filler metal droplets for welds produced using reactive shielding gases are spread out and this resulted in larger impingement areas and weld widths (Ref. 17).

Between welding powers of 7.5 and 9 kW, the filler metal transfer mode for all shielding gases was predominantly spray transfer. However, as shown in Fig. 12, the individual filler metal droplets were swung around in a helical path as they detached from the tip of the electrode wire and propelled across the welding arc to the weld pool. This is identified as swinging spray transfer mode, which is considered to be a transitional stage between spray and rotational transfer modes (Ref. 27). For the GMA welds produced using argon shielding gas, the swinging spray transfer mode can facilitate higher welding speeds since it reduces the vertical velocity component of the molten filler metal droplets to lessen their ability to gouge the weld pool enlarges the impingement area on the top surface of the weld pool, and prevents the molten filler metal droplets from always hitting the leading edge of the gouged weld pool. This reduces the momentum of the molten weld metal toward the rear of the weld pool, thereby suppressing the tendency for humping to occur until high welding speeds are used (Ref. 17).

As shown in Fig. 12, above 9 kW welding power, the welding wire melts and forms a long liquid string that is still attached to the solid tip of the electrode. This molten filler metal string is indiscriminately coiled and violently swung around inside the shroud of the welding arc. This is identified as the rotational transfer mode, which typically occurs at power levels higher than those obtained for spray transfer (Refs. 28, 29). The direction of rotation of the molten filler metal string is random even when identical welding parameters are used (Ref. 30). In general, the rotational transfer mode

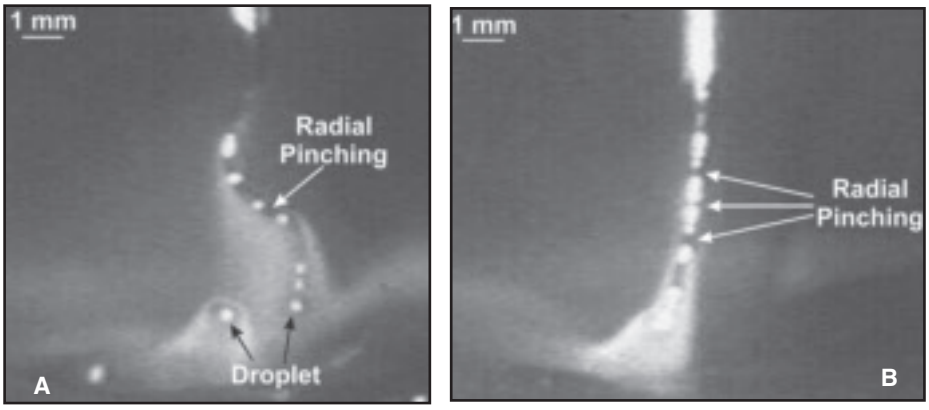

Fig. 16 — The LaserStrobe™ video images showing the effect of radial pinch instability on the molten filler metal string during GMA welding of steel using argon shielding gas and 11 kW welding power. Depending on the orientation, the molten filler metal string can be viewed as dark field in A or a bright field in B.

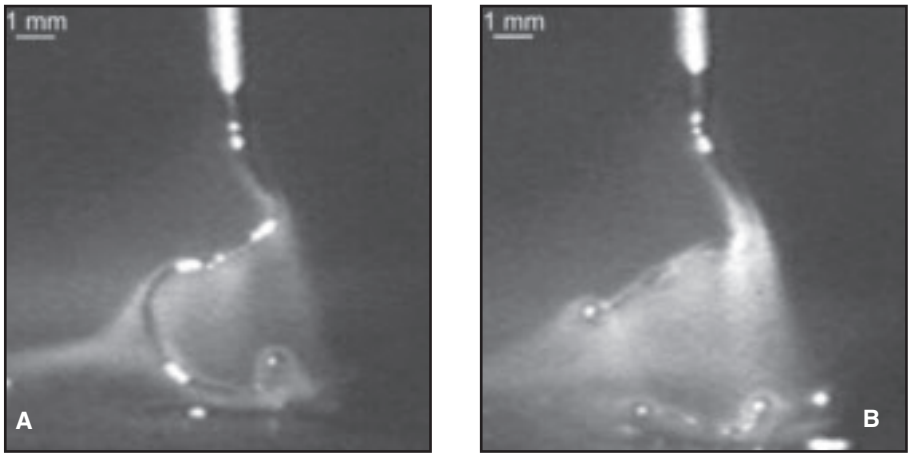

Fig. 17 — The breakup of the long filler metal string as a result of short circuiting with the surface of the workpiece.

produces the highest level of filler metal deposition rates when compared to other transfer modes (Refs. 1–4, 28, 29).

From the results shown in Figs. 11 and 12, the occurrence of the humping weld defect coincides with the spray transfer mode. When using the reactive shielding gases, however, the transition to rotational transfer mode coincided with the appearance of the discontinuous weld bead defect. Thus, for reactive shielding gases, the type of high-speed weld bead defect observed appears to be related to the filler metal transfer modes. To further understand the formation of the discontinuous weld bead defect, a more detailed examination of the rotational transfer mode was undertaken.

Rotational Transfer Mode during GMA Welding

From the images in Fig. 12, rotational metal transfer mode occurred when the welding power was greater than 9 kW. The filler metal droplets can be seen to detach from the tip of the molten string similar to that previously reported for rotational transfer mode in GMA welding (Refs. 27–30). The flight path of the detached droplets was typically along the same line as the molten string. However, since the string rotated in a random manner, the droplets were erratically deposited over the surface of the weld pool. For instance, the image of an argon-shielded GMA weld at 11 kW welding power in Fig. 13 shows that some of the molten filler metal droplets were detached in the welding direction and transferred to the front portion of the weld pool. In addition, the swinging action of the molten filler metal string resulted in some of the droplets having an upward flight path prior to falling back down to the weld pool. The swinging action of the molten filler metal string and the erratic deposition of the molten filler metal droplets generated spatter on the surface of the workpiece adjacent to the weld bead — Fig. 7. Also visible in this and other images is a halo of glowing gas around each metal droplet and a glowing comet tail trailing behind the droplets. This may be evidence of interactions between vaporizing elements from the metal droplets such as Mn and the ionized high-

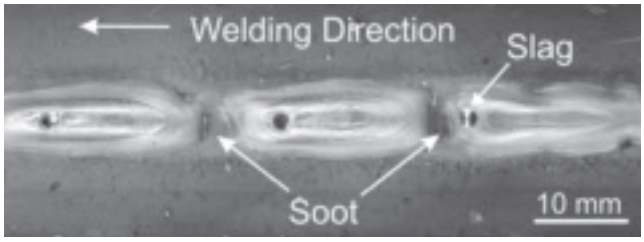

Fig. 18 — The top surface of a GMA weld with discontinuous weld bead defect immediately after welding.

Fig. 20 — LaserStrobe™ video image that shows the length of the depression formed.

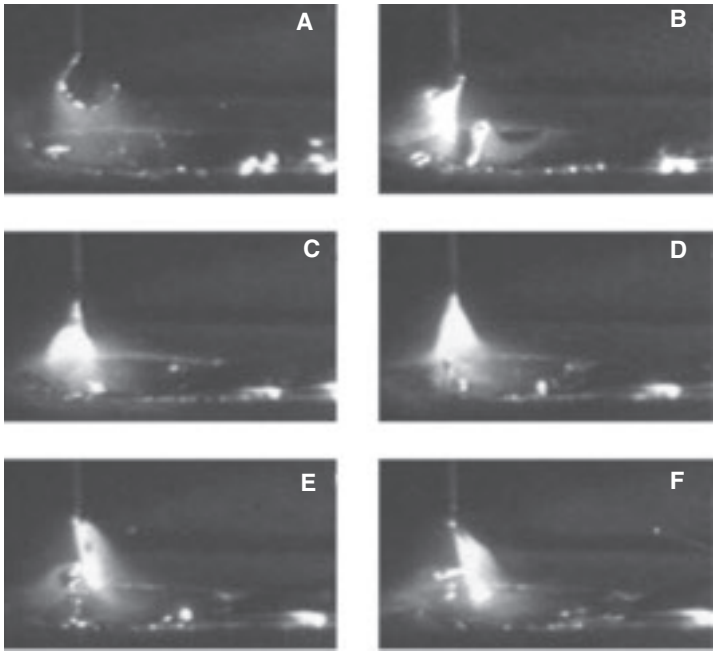

Fig. 19 — A sequence of six LaserStrobe™ video images showing the formation of a discontinuous weld bead defect.

velocity plasma stream in the arc.

In addition to the droplets detaching from the tip of the filler metal string, the molten filler metal string was also seen to be broken up into longer fragments that fell directly into the weld pool. While metal transfer by droplet detachment has been observed and reported in previous publications of rotational transfer mode in GMAW (Refs. 27–30), this is the first time that metal transfer by fragmentation or complete detachment of the long molten metal string on the end of the electrode has been observed. An image of the fragmented molten filler metal string is shown in Fig. 14. Detachment of the long string fragment shortened the molten filler metal string considerably. In this case, the original molten string was cut in half as a result of the breakup. At the new tip of the string, a new molten filler metal droplet was forming and would be detached very shortly.

Fragmentation of the molten filler metal string was not restricted to argon-shielded welds. Similar LaserStrobe™ video images showing the breakup of a long molten filler metal string were also found for welds produced using the reactive shielding gases. For each shielding gas and welding power combination, 600 LaserStrobe™ video images were examined to determine the number of frames that clearly showed the fragment of the molten filler metal string. The results were then divided by 600 and converted to a percentage to represent the probability of having the long molten filler metal string breaking up into fragments. The probability of having a fragmented string when using each shielding gas at 10, 11, and 12 kW welding power are plotted in Fig. 15. From these results, the molten filler metal string that exists during rotational transfer mode occasionally broke up into long fragments rather than droplets. The probability of breaking up into string fragments was highest for argon followed by MMG™ and TIME™ shielding gases, respectively. For GMA welds produced using TIME™ shielding gas, the breakup of the molten filler metal string is constant at about 4% and relatively independent of the welding power. Meanwhile, for welds produced using MMG™ shielding gas, there is a slight reduction in the frequency of breakup of the long molten filler metal string into fragments at lower welding powers. Lastly, the welding power had the most influence when using argon shielding gas; the higher the welding power, the more frequent was the breakup of the long molten filler metal string. In fact, on increasing the welding power from 10 to 12 kW (20% increase), the frequency of string fragmentation more than doubled; i.e., it increased from 6 to 13%.

If it is assumed that the molten filler metal string can be approximated as a fluid cylinder, then the GMAW filler metal transfer modes can be attributed to influences of either the radial pinch or kink instabilities (Ref. 27). The radial pinch instability of the fluid cylinder is responsible for the formation and the detachment of molten filler metal droplets in the globular and spray transfer modes during GMA welding. Meanwhile, the swinging action of the molten filler metal string observed in rotational filler metal transfer mode is caused by the effect of the kink instability on the fluid cylinder. This particular instability can be described geometrically as the collapse of a straight fluid cylinder into a spiral shape (Ref. 27). During rotational transfer mode, however, the radial pinch instability is also present and is responsible for the detachment of droplets from the tip of the molten string in rotational transfer mode as shown in the LaserStrobe™ video image of Fig. 13. Thus, in rotational transfer mode, the effects of radial pinch instabilities on the fluid cylinder are still present, but not dominant.

Figure 16 shows two LaserStrobe™ video images of the molten filler metal string at different times during GMA welding of steel using argon shielding gas and 11 kW welding power. In Fig. 16A, the molten filler metal string is at an orientation such that the specular reflection of the N_2 laser light toward the CCD camera does not occur. As a result, the string in this image appears mostly as a dark field. Meanwhile, in Fig. 16B, the molten filler metal string is a bright field since its orientation allows the N_2 laser to be reflected back to the CCD camera of the LaserStrobe™ video imaging system.

In Fig. 16A, the formation and detachment of molten filler metal droplets from the tip of the filler metal string are clearly observed. The spherical-shaped droplets

reflect the N_2 laser light back to the CCD camera. As a result, a bright spot on the surface of each droplet is clearly observed in the image. Although the string is seen as a dark field because the curved surface of the string does not allow the reflection of the N_2 laser back to the CCD camera, there are a few visible bright spots in Fig. 16A. The bright spots are simply an indication that the N_2 laser light is being reflected back to the CCD camera at these locations by specular reflections off a spherical shape similar to the molten filler metal droplets. In other words, these bright spots represent the swellings that occur along the length of the molten filler metal string. Similar to the formation of the droplets, the swellings are formed by radial pinching of the molten filler metal string into thinner necking regions. The thinning of these necking regions will ultimately result in breakup of the long molten filler metal string into fragments as seen in Fig. 14.

In Fig. 16B, a major portion of the molten filler metal string is seen as a bright field. At this instant in time, the molten filler metal string had an orientation that allowed specular reflection of the N_2 laser light back to the CCD camera. However, there are several dark segments along the bright length of the molten filler metal string. The surface profile at the dark segments must be different than the rest of the molten filler metal string in order to cut off the specular reflection of the N_2 laser light back to the CCD camera. If these dark segments have a swelling or a spherical surface profile, then a bright spot similar to that observed for a droplet would be visible. However, this is not the case. As indicated in Fig. 16B, these dark segments occur in between the bright segments of the molten filler metal string. From these observations, the dark portions must have pinched or necking surface profiles, a direct result of a radial pinch instability.

From the images in Fig. 16A, B, although it is not dominant, the radial pinch instability is present during rotational transfer mode. In addition to producing and detaching the droplets at the tip, the radial pinch instability also causes necking to form along the length of the molten filler metal string. The thinning of these necking regions will eventually break up the molten filler metal string into fragments as seen in Fig. 14. The fragment of the molten filler metal string shortens the molten metal string considerably. In addition to necking, the long molten filler metal string can also be broken up into fragments as the string momentarily touches the surface of the workpiece. This phenomenon is illustrated by the images in Fig. 17.

Table 3 — The Voltage and the Measured Welding Current at 10, 11, and 12 kW for Argon, MMG™, and TIME™ Shielding Gases

	Argon		MMG™		TIME™	
	Voltage (V)	Avg. Current (A)	Voltage (V)	Avg. Current (A)	Voltage (V)	Avg. Current (A)
10 kW	32.5	306.5	34.5	288.0	35.5	278.4
11 kW	33.0	326.1	35.0	315.0	36.0	306.7
12 kW	36.0	333.7	37.3	326.9	38.5	311.5

The LaserStrobe™ video images shown in Fig. 17A and B were taken approximately 33 ms apart. In Fig. 17A, a long molten filler metal string was violently swung around with the end portion of the string about to touch the surface of the workpiece. In Fig. 17B, the molten filler metal string was broken up into two segments. During the 33-ms time interval between the first and the second images, the long molten filler metal string apparently touched the leading edge of the weld pool. This contact momentarily created a short circuit, which resulted in a surge of welding current. Since the molten filler metal string was in liquid form, a small current surge was needed to eliminate the short circuiting. In the process of eliminating the short circuiting, the molten filler metal string was shattered into fragments as shown in Fig. 17B.

The Soot Layer

A layer of rust-colored soot was observed covering the bottom surface of many of the depressions of the discontinuous weld bead defect. The presence of a contaminant layer can prevent molten weld metal from refilling the gouged region of the weld pool by preventing contact and wetting at the fusion boundary. As this could also contribute to the formation of the depressions that break up the weld bead into segments, further examination of the soot layer at the bottom of the depression and its effects on the formation of the discontinuous weld bead defect was undertaken.

Figure 18 shows the as-welded top surface of a GMA weld with the discontinuous weld bead defect. The surface of the workpiece adjacent to the weld bead is covered with a thick layer of rust-colored soot, while the good weld bead segments are relatively clean. As noted in Fig. 18, the dark spots formed on the top surface at the end of each good weld bead segment were found to be a $(Mn,Si)_xO_y$ glassy slag. In addition, there was a thin layer of soot completely covering the bottom surface of the depressions of the discontinuous weld bead. The chemical composition of the soot on the top surface of the adjacent workpiece and the soot covering the bottom surface of the depression were analyzed using a LEO FESEM 1530 field emission scanning electron microscope equipped with an EDX analysis system. Since the soot just covered the top surface of the workpiece, the scanning electron microscope was set at 15 keV to minimize the interaction volume between the electrons and the analyzed material (Ref. 31). The small interaction volume ensured that the elements detected during the chemical analysis belonged to the soot. The elemental constituents of the soot covering the top surface of the workpiece adjacent to the weld bead were identified as Fe, Mn, Si, Zn, and oxygen. Since the ER70S-6 electrode wire has a high content of deoxidizers such as Mn and Si (Table 1), it is not unexpected to find these elements in the chemical composition of the soot. During welding, it is thought that the Mn and Si from the electrode wire were vaporized inside the welding arc. As the welding gun moved forward, the Mn and Si metal vapors oxidized and condensed on the surface of the workpiece adjacent to the weld bead. Meanwhile, as shown in Fig. 18, the good weld segments were clear of any soot since the weld bead was at higher temperatures during the time period when the metal vapors condensed.

An EDX analysis was also performed on the soot layer covering the bottom surface of the depression — Fig. 18. Using the same setup on the scanning electron microscope, the elements detected by this EDX analysis were Fe, Mn, Si, and oxygen, which are similar to those elements found in the rust-colored soot formed on the surface of the workpiece adjacent to the weld bead. From the results of the chemical analysis, the soot, which covers the bottom surface of the depressions of a discontinuous weld bead defect, was chemically similar to the common welding soot that typically forms on the cooler metal surface adjacent to the weld bead. As previously discussed, the shallow HAZ suggests that there was less sensible heat input at the depression — Fig. 9. As a result, the surface of the depression was cooler than the adjacent good segments of the weld bead. The Mn and Si metal vapors condensed over the bottom surface of the depression just as they condensed on

the surface of the workpiece adjacent to the weld bead. Since the soot layer was produced from the metal vapors that oxidized and condensed at some distance behind the welding arc, it was not present inside the weld pool to prevent the molten weld metal from refilling the gouged region. Thus, the observed layer of soot is not responsible for the formation of the depressions in the discontinuous weld bead defect.

The Role of Rotational Transfer Mode in Forming the Discontinuous Weld Bead Defect

The LaserStrobe™ video imaging system was used to observe the formation of a discontinuous weld bead defect made at 40 mm/s welding speed when using MMG™ shielding gas, ER70S-6 electrode wire, and 10 kW welding power. Figure 19 contains a sequence of six video images each 33 ms apart detailing the events that took place during the formation of a discontinuous weld bead defect. In Fig. 19A, a long molten filler metal string is clearly visible with the molten filler metal droplets that are being formed, detached, and transferred to the weld pool from the tip of the string. As previously mentioned, in the rotational transfer mode regime, the radial pinch instability that acts on the molten filler metal string is responsible for the formation and detachment of the droplets (Ref. 27). This particular instability is also capable of producing necking at various places along the length of the molten filler metal string. In Fig. 19A, the necking regions are seen as the dark rings along the length of the molten filler metal string. The thinning of these necking regions will eventually break up the long molten filler metal string into fragments as shown in Fig. 19B. With the breakup, the original molten filler metal string and the arc length are shortened as compared to those in Fig. 19A.

In Fig. 19B, the end of the detached fragment is clearly visible above the surface of the weld pool while the remaining portion of the original molten filler metal string is still attached to the solid electrode wire. However, in the 33-ms time period between Fig. 19B and C, the remaining portion of the original string has broken off from the tip of the solid electrode wire and transferred to the weld pool. As is clearly evident in Fig. 19C, during this time period, transfer of molten filler metal to the weld pool does not occur. In fact, a new molten filler metal droplet is beginning to form at the tip of the electrode in Fig. 19C. With the formation of a new molten filler metal droplet at the tip of the solid electrode wire, the arc length is apparently the longest in the sequence as compared to the arc lengths of Fig. 19B and C, respectively.

In Fig. 19C, the welding arc behaves as if it is an autogenous welding process. As may be seen in Fig. 19A–D, the width of the weld pool remains consistently the same. This suggests that the heat input from the welding arc has not been influenced by the breakup and the detachment of the long molten filler metal string. As a result, the heat generated by the welding arc continues to melt and to penetrate the original surface of the workpiece although the transfer of molten filler metal does not occur.

In Fig. 19D, one molten filler metal droplet is seen momentarily before touching the top surface of the weld pool. This may be the molten filler metal droplet, which is noted in the previous image of Fig. 19C. In the 33-ms time period between Fig. 19B and C, there is a large addition of molten filler metal to the weld pool due to the detachment of a long molten filler metal string. Meanwhile, for the same time period between Fig. 19C and D, there is approximately one filler metal droplet transferred to the weld pool. This is a considerable reduction in the amount of filler metal transferred. The reduced transfer of molten filler metal may also extend from the Fig. 19D to Fig. 19E time period. After the detachment of a long molten filler metal string, the GMA welding process temporarily switches back to the early stage of spray transfer mode as evidenced by the formation and the detachment of a molten filler metal droplet. Eventually, a new molten filler metal string begins to form again in Fig. 19E and rotational transfer mode is resumed with the long molten filler metal string as illustrated in Fig. 19F. For the 67-ms time period starting from Fig. 19C and ending at Fig. 19E, there is a large reduction in the amount of filler metal transferred into the weld pool. During this time period, the welding arc continued to melt and to penetrate the workpiece similar to an autogenous welding process. As a result, the depression of a discontinuous weld bead defect should have the same penetration depth as the good weld segments. As previously discussed, this was one of the observed geometric features of the depression region of a discontinuous weld bead defect. However, because of the reduced amount of the filler metal transferred, the HAZ at the depression is smaller compared to the HAZ under the good weld bead segments — Fig. 9.

At 40 mm/s welding speed and 67-ms time period, the linear distance traveled by the welding arc along the weld joint is approximately 2.7 mm. Over this distance, the amount of filler metal transferred to the weld pool has been drastically reduced. There will not be enough molten weld metal to form a proper weld bead profile. As a result, a depression separating the good weld bead segments will form. Theoretically, the length of the depression as measured in the welding direction should be approximately 2.7 mm. Figure 20 is a LaserStrobe™ video image showing the length of the depression that was formed during the sequence of images in Fig. 19. As indicated, the length of the depression is approximately 2.7 mm, which is equal to the linear distance over which the amount of filler metal transferred to the weld pool was drastically reduced. These images suggest that inconsistent filler metal transfer rate during rotational transfer mode causes the formation of the depression in discontinuous weld bead defect.

For GMA welds produced using argon shielding gas, the discontinuous weld bead defect did not occur at higher welding powers although the filler metal transfer mode was rotational. One possible explanation is the frequent fragment detachments from the long molten filler metal string with argon shielding gas as shown in Fig. 15. The arc lengths of argon-shielded GMA welds were about twice the arc lengths of welds produced using the reactive shielding gas (Ref. 17). In addition, the surface tension of molten steel in argon shielding gas will be higher than that in reactive shielding gases (Ref. 32). Because of the long arc length and the high surface tension, the length of the molten filler metal string will also be longer compared to those present when using reactive shielding gases.

For each GMA weld, the voltage and the wire feed speed were normally set prior to welding. In the present study, during welding, the current was measured using the previously described data-acquisition system. The voltage and the average welding current for different welding powers and shielding gas combinations are shown in Table 3. In general, the welds produced using argon shielding gas had lower voltage settings, but larger welding currents, than those produced using the reactive shielding gases. With high welding currents, the radial pinch force would be stronger since the electromagnetic force that generated the pinch force is a function of the welding current (Refs. 2, 29). As a result, the detachments of molten filler metal droplets and more importantly, the fragments, occurred more frequently for argon shielding gas — Fig. 15. With the long molten filler metal string and the more frequent fragment detachments, the filler metal deposition rate will be more consistent. In other words, the time period in which the molten filler metal is not transferred to the weld pool is relatively short or nonexistent. As a result,

the discontinuous weld bead defect does not occur at higher welding powers. Instead, the humping phenomenon is the limiting factor that prevents achievement of higher welding speeds.

With the higher welding powers and rotational filler metal transfer, the welding speeds for GMA welds produced using reactive shielding gases are limited by the formation of the discontinuous weld bead defect. From experimental observations, the inconsistent amount of molten filler metal deposited during rotational transfer mode is the cause of the discontinuous weld bead defect. This inconsistent filler metal transfer rate is caused by the erratic breakup of the long molten filler metal string that typically exists in rotational transfer. After the detachment of the fragment, time is required for the string to reestablish. Meanwhile, at high welding speeds, the welding arc proceeds along the weld joint as if it is an autogenous welding process. The heat generated by the autogenous welding arc consistently maintains the weld width and the penetration depth. However, the lack of filler metal transfer during this time period creates a depression that breaks up the otherwise good weld bead. Consequently, the discontinuous weld bead defect is formed.

Conclusions

Detailed observations of the sequence of events taking place during the formation of weld bead defects during high-speed bead-on-plate gas metal arc welding of plain carbon steel using ER70S-3 and ER70S-6 electrode wires, and Ar and two different reactive shielding gases have been made. At welding powers between 5 and 9 kW, spray metal transfer occurred and the welding speed was limited by the onset of the periodic humping weld bead defect.

For GMA welds produced with argon shielding gas, there was a small increase in the critical welding speed at which humping began as the welding power was increased from 5 to 9 kW. When the welding power was further increased from 9 to 12 kW, however, the filler metal transfer mode was observed to go from streaming to swinging spray transfer and the critical welding speed at which humping was observed remained constant at about 15 mm/s.

When using the reactive shielding gases, MMG™ and TIME™, the filler metal transfer mode changed from spray to rotational transfer when the welding power was increased above 9 kW. In this case, the critical welding speed of the GMA welds produced using rotational transfer mode and reactive shielding gases was defined by the onset of a new aperiodic high-speed weld bead defect that was identified and defined as a discontinuous weld bead defect. Above 9 kW welding power, the discontinuous weld bead defect always occurred at welding speeds greater than 22 mm/s independent of the welding power. The results indicated that nominal wire composition did not appear to play a significant role in the formation of periodic humping or the aperiodic discontinuous weld bead defects.

The aperiodic discontinuous weld bead defect is distinctly different from the periodic humping weld bead defect and has never before been reported in the open literature. This weld bead defect can be described as the breakup of a good GMA weld bead by the aperiodic or intermittent formation of valleys or depressions where melting of the base metal occurred but no filler metal was deposited. The good weld bead segments of discontinuous weld beads had well-rounded fusion boundaries without the finger penetration weld pool profile characteristic of GMA welds made using spray transfer mode. This good weld bead was broken up into segments by the aperiodic occurrence of filler-metal-free depressions that were very similar to a severely gouged autogenous weld bead produced using high welding power but no filler metal.

The formation of the discontinuous weld bead defect has been explained as the consequence of the inconsistent transfer of the molten filler metal from the electrode wire to the weld pool when welding with reactive shielding gases in rotational transfer mode. LaserStrobe™ video images of the rotational transfer mode showed the filler metal detaching from a long molten metal string on the end of the electrode that was violently swung around inside the shroud of the welding arc. Due to the radial pinching or necking that occurred along the length of the molten string, the filler metal was transferred either as droplets or as long fragments into the weld pool. On occasion, the long molten filler metal string momentarily touched the weld pool and broke up into fragments. Fragmentation or complete detachment of the molten filler metal string during rotational transfer mode has not been observed or previously reported in the open literature. This fragmentation of the long molten metal string on the end of the electrode wire temporarily disrupts the transfer of the molten filler metal into the weld joint. Since the welding arc is moving forward at high welding speed, the disruption in filler metal transfer creates a depression, a region of the weld bead where no filler metal has been deposited, and breaks up the normally good GMA weld bead to form the aperiodic discontinuous weld bead defect. The random fragmentation of the molten metal string on the end of the electrode during rotational metal transfer has not been previously observed or reported.

For the GMAW process, the periodic humping weld defect and the aperiodic discontinuous weld bead defect limit the usable welding speed in spray and rotational transfer modes, respectively. The discontinuous weld bead defect is distinctly different from humping and is the direct result of inconsistent filler metal deposition during rotational transfer. For the first time, the manner in which the molten filler metal is transferred from the electrode across the welding arc to the weld pool during the GMAW process has been shown to be very influential in the formation of high-speed defects such as humping and discontinuous weld beads.

Acknowledgments

This work was supported by Natural Sciences and Engineering Research Council of Canada (NSERC), Ontario Research and Development Challenge Fund (ORDCF), and its partners Alcan International, Babcock & Wilcox, Canadian Liquid Air Ltd., CenterLine (Windsor) Ltd., John Deere, Magna International Inc., and Ventra. Loan of robotic GMA welding equipment by Lincoln Electric Co. of Canada Ltd. and Fanuc Robotics Canada Ltd. is gratefully acknowledged. The TIME™ shielding gas used in this study was supplied by BOC Gas.

References

1. Cary, H. B. 2002. *Modern Welding Technology*. 5th ed., Toronto, Ont., Canada: Prentice Hall Canada Inc. p. 477.

2. *Welding Handbook*, Vol. 1, Welding Science and Technology. 1991. 8th ed., Miami, Fla.: American Welding Society. p. 50.

3. *ASM Handbook* — Welding, Brazing and Soldering, Vol. 6. 1993. Davies et al. eds., Materials Park, Ohio: ASM International.

4. *Welding Handbook*, Vol. 2, Welding Processes. 1991. 8th ed., Miami, Fla.: American Welding Society. p. 112–116.

5. Nguyen, T. C., Weckman, D. C., Johnson, D. A., and Kerr, H. W. 2006. High speed fusion weld bead defects. *Science and Technology of Welding and Joining* 11(6): 618–633.

6. Soderstrom, E., and Mendez, P. 2006. Humping mechanisms present in high speed welding. *Science and Technology of Welding and Joining* 11(5): 572–579.

7. Bradstreet, B. J. 1968. Effect of surface tension and metal flow on weld bead formation. *Welding Journal* 47(6): 314-s to 322-s.

8. Nishiguchi, K., Matsuyama, K., Terai, K., and Ikeda, K. 1975. Bead formation in high speed gas-shielded metal-arc welding. *Proc. 2nd Int. Symp. of the Japan Welding Soc. on 'Advanced Welding Technology*,' Osaka, Japan. Japan Welding Society, Paper 2-2-(10).

9. Nishiguchi, K., and Matsunawa, A. August 1975. Gas metal arc welding in high pres-

sure atmospheres — arc characteristics and bead formation mechanisms. *Proc. 2nd Int. Symp. of the Japan Welding Soc. on 'Advanced Welding Technology,'* Osaka, Japan. Japan Welding Society, Paper 2-2-(5).

10. Yamamoto, T., and Shimada, W. 1975. A study on bead formation in high speed TIG arc welding at low gas pressure. *Proc. Advanced Welding Technology — 2nd Int. Symp. of the Japan Welding Soc. on 'Advanced Welding Technology*,' Osaka, Japan. Japan Welding Society, Paper 2-2-(7).

11. Savage, W. F., Nippes, E. F., and Agusa, K. 1979. Effect of arc force on defect formation in GTA welding. *Welding Journal* 58(7): 212-s to 224-s.

12. Hiramoto, S., Ohmine, M., Okuda, T., and Shinmi, A. 1987. Deep penetration welding with high power CO_2 laser. *Proc. Int'l Conf. on 'Laser Advanced Material Processing — Science and Application,'* Osaka, Japan. High Temp. Society of Japan and Japan Laser Processing Society, pp. 157–162.

13. Albright, C. E., and Chiang, S. 1988. High-speed laser welding discontinuities. *Journal of Laser Applications* 1(1): 18–24.

14. Tsukamoto, S., Irie, H., Inagaki, M., and Hashimoto, T. 1983. Effect of focal position on humping bead formation in electron beam welding. *Trans. of National Research Inst. for Metals* 25(2): 62–67.

15. Tsukamoto, S., Irie, H., Nagaki, M., and Hashimoto, T. 1984. Effect of beam current on humping bead formation in electron beam welding. *Trans. of National Research Inst. for Metals* 26(2): 133–140.

16. Tomie, M., Abe, N., and Arata, Y. 1989. Tandem electron beam welding (Report IX) — high speed tandem electron beam welding. *Trans. of Japan Welding Research Inst.* 18(2): 175–180.

17. Nguyen, T. C., Weckman, D. C., Johnson, D. A., and Kerr, H. W. 2005. The humping phenomenon during high-speed gas metal arc welding. *Science and Technology of Welding and Joining* 10(4): 447–459.

18. Shimada, W., and Hoshinouchi, S. 1982. A study on bead formation by low pressure TIG arc and prevention of undercut bead. *Journal of Japan Welding Soc.* 51(3): 280–286.

19. Mendez, P. F., and Eagar, T. W. 1998. Magnitude scaling of free surface depression during high current TIG arc welding. *Proc. 5th Int'l Conf. Trends in Welding Research*, Pine Mountain, Ga., J. M. Vitek, S. A. David, J. A. Johnson, H. B. Smartt, and T. DebRoy, eds., pp. 13–18, Materials Park, Ohio: ASM International.

20. Mendez, P. F., and Eagar, T. W. 2001. Estimation of the characteristic properties of the weld pool during high productivity arc welding. *Proc. Mathematical Modelling of Weld Phenomena 5 Conf.*, eds. H. Cerjak and H. K. D. H. Bhadeshia, pp. 67–94, London, UK: Inst. of Materials.

21. Mendez, P. F., and Eagar, T. W. 2003. Penetration and defect formation in high-current arc welding. *Welding Journal* 82(10): 296-s to 306-s.

22. Gratzke, U., Kapadia, P. D., Dowden, J., Kross, J., and Simon, G. 1992. Theoretical approach to the humping phenomenon in welding processes. *Journal of Physics D: Applied Physics* 25(11): 1640–1647.

23. Paton, E. O., Mandel'berg, S. L., and Sidorenko, B. G. 1971. Certain special features of the formation of welds made at high speeds. *Avt. Svarka* 24: 1–6.

24. Nguyen, T. C. 2005. *Weld Defects in High-Speed Gas Metal Arc Welding,* PhD thesis. Waterloo, Ont., Canada: University of Waterloo.

25. LaserStrobe™ Model 4Z — Operation Manual. 1999. Idaho Falls, Idaho: Control Vision Inc.

26. Vander Voort, G. F. 1999. *Metallography Principles and Practice.* Materials Park, Ohio: ASM International.

27. Ushio, M., Ikeuchi, K., Tanaka, M., and Seto, T. 1993. Effects of shielding gas composition on metal transfer phenomena in high current GMA welding. *Trans. Japan Welding Research Inst.* 22(1): 7–12.

28. Lyttle, K. A. 1983. GMAW – A versatile process on the move. *Welding Journal* 62(3): 15–23.

29. Lancaster, J. F. ed. 1984. *The Physics of Welding.* Willowdale, Ont., Canada: Pergamon Press Canada Ltd.

30. Yamamoto, H., Harada, S., and Yamamoto, Y. 1990. Arc characteristics and metal transfer in high current MAG welding — effect of shielding gas composition on metal transfer. *Proc. 5th JWS Int'l Symposium — Advanced Technology in Welding, Material Processing and Evaluation*, Japan Welding Society, Tokyo, Japan. pp. 115–120.

31. Goldstein, J. I., Newbury, D. E., Echlin, P., Joy, D. C., Romig Jr., A. D., Lyman, C. E., Fiori, C., and Lifshin, E. 1990. *Scanning Electron Microscopy and X-Ray Microanalysis*, 2nd ed. New York, N.Y.: Kluwer Academic & Plenum Publishers. pp. 79–90.

32. Subramanian, S., and White, D. R. 2001. Effect of shielding gas composition on surface tension of steel droplets in a gas-metal-arc welding arc. *Metallallurgical & Materials Transactions B* 32B(2): 313–318.

Preparation of Manuscripts for Submission to the *Welding Journal* Research Supplement

All authors should address themselves to the following questions when writing papers for submission to the Welding Research Supplement:

- ◆ Why was the work done?
- ◆ What was done?
- ◆ What was found?
- ◆ What is the significance of your results?
- ◆ What are your most important conclusions?

With those questions in mind, most authors can logically organize their material along the following lines, using suitable headings and subheadings to divide the paper.

1) **Abstract.** A concise summary of the major elements of the presentation, not exceeding 200 words, to help the reader decide if the information is for him or her.

2) **Introduction.** A short statement giving relevant background, purpose, and scope to help orient the reader. Do not duplicate the abstract.

3) **Experimental Procedure, Materials, Equipment.**

4) **Results, Discussion.** The facts or data obtained and their evaluation.

5) **Conclusion.** An evaluation and interpretation of your results. Most often, this is what the readers remember.

6) **Acknowledgment, References and Appendix.**

Keep in mind that proper use of terms, abbreviations, and symbols are important considerations in processing a manuscript for publication. For welding terminology, the *Welding Journal* adheres to AWS A3.0:2001, *Standard Welding Terms and Definitions.*

Papers submitted for consideration in the Welding Research Supplement are required to undergo Peer Review before acceptance for publication. Submit an original and one copy (double-spaced, with 1-in. margins on 8 ½ x 11-in. or A4 paper) of the manuscript. A manuscript submission form should accompany the manuscript.

Tables and figures should be separate from the manuscript copy and only high-quality figures will be published. Figures should be original line art or glossy photos. Special instructions are required if figures are submitted by electronic means. To receive complete instructions and the manuscript submission form, please contact the Peer Review Coordinator, Erin Adams, at (305) 443-9353, ext. 275; FAX 305-443-7404; or write to the American Welding Society, 550 NW LeJeune Rd., Miami, FL 33126.